Tensor Approach for Eigenvector-Based Multi-Dimensional Harmonic Retrieval

Weize Sun, Hing Cheung So, *Senior Member, IEEE*, Frankie Kit Wing Chan, and Lei Huang, *Member, IEEE*

***Abstract*—In this paper, we propose an eigenvector-based frequency estimator for R-dimensional (R-D) sinusoids with $R \geq 2$ in additive white Gaussian noise. Our underlying idea is to utilize the tensorial structure of the received data and then apply higher-order singular value decomposition (HOSVD) and structure least squares (SLS) to perform estimation. After obtaining the tensor-based signal subspace from HOSVD, we decompose it into a set of single-tone tensors from which single-tone vectors can be constructed by another HOSVD. In doing so, the R-D multiple sinusoids are converted to a set of single-tone sequences whose frequencies are individually estimated according to SLS. The mean and variance of the frequency estimator are also derived. Computer simulations are also included to compare the proposed approach with conventional R-D harmonic retrieval schemes in terms of mean square error performance and computational complexity particularly in the presence of identical frequencies.**

***Index Terms*—Array processing, multi-dimensional harmonic retrieval, parameter estimation, subspace method, tensor algebra.**

I. Introduction

MANY important problems in communications and signal processing can be cast into the harmonic retrieval (HR) [1] formulation where the parameters of a discrete harmonic mixture are needed to estimate from a set of observations taken along time, frequency or space. In this work, we address the topic of R-dimensional (R-D) HR where $R \geq 2$ with single and multiple snapshots. Representative application examples are joint direction-of-arrival and polarization estimation using electromagnetic vector sensor [2], wireless communication channel estimation [3], [4], nuclear magnetic resonance spectroscopy [5], [6] as well as multiple-input multiple-output radar imaging [7], [8].

Subspace approach is a standard choice for multi-dimensional HR because it strikes a good balance between estimation accuracy and computational complexity. The underlying idea of the subspace methodology is to separate the data into signal and noise subspaces. For 2-D data, it is usually achieved by singular value decomposition (SVD) of the raw data matrix or eigenvalue decomposition (EVD) of the sample covariance matrix, and the parameters of interest are then extracted from the corresponding eigenvectors, singular vectors, eigenvalues or singular values. For higher-dimensional data, it is more natural to store and manipulate them using tensors [9]–[11] where the subspace decomposition can be obtained by the higher-order singular value decomposition (HOSVD). Generally speaking, tensor-based algorithms are superior to the matrix-based counterparts in terms of estimation performance in handling signals whose dimensions are larger than 2, although the former have a higher computational load.

State-of-the-art subspace methods for R-D HR include estimation of signal parameters via rotational invariance technique (ESPRIT) [12]–[16], multi-dimensional folding (MDF) [17], [18] and principal-singular-vector utilization for modal analysis (PUMA) [19], [20]. Although the PUMA approach is computationally attractive and its mean square error performance can attain the benchmark of Cramér-Rao lower bound (CRLB) in additive white Gaussian noise, it may not work well when there are identical frequencies in one or more dimensions. On the other hand, the ESPRIT and MDF schemes can handle identical frequency scenarios but they may not be able to achieve optimum estimation performance. Their limitations motivate us to devise a new R-D HR method which possesses the advantages of the conventional schemes. Our proposal is an eigenvector-based approach with the use of the HOSVD and structured least squares (SLS) technique. HOSVD is first applied to the received data tensor to obtain the signal subspace which corresponds to a sum of multiple sinusoids. Single-tone vectors are then constructed from the signal subspace by another HOSVD via forming a set of sub-tensors based on a suboptimum selection criterion. SLS is then utilized to provide accurate frequency estimation from all 1-D vectors in a separable manner. In doing so, frequency pairing is automatically achieved.

The rest of the paper is organized as follows. In Section II, we first introduce the notation and then formulate the problem of R-D HR in the presence of white Gaussian noise. By exploiting the subspace methodology and tensor algebra, the proposed eigenvector-based estimation algorithm is developed in Section III. In Section IV, the mean and variance of the frequency estimator are derived and it is proved that the frequency estimates are approximately unbiased. In Section VI, simulation results are included to evaluate the performance of the proposed approach by comparing with the ESPRIT [14], [15] and MDF [18] algorithms as well as CRLB in identical frequency conditions. Finally, conclusions are drawn in Section V.

Manuscript received October 08, 2012; revised February 02, 2013; accepted April 03, 2013. Date of publication April 19, 2013; date of current version June 07, 2013. The associate editor coordinating the review of this manuscript and approving it for publication was Prof. Sofiene Affes. The work described in this paper was supported by a grant from the NSFC/RGC Joint Research Scheme sponsored by the Research Grants Council of the Hong Kong and the National Natural Science Foundation of China (Project No.: N_CityU 104/11, 61110229/61161160564).

W. Sun, H. C. So, and F. K. W. Chan are with the Department of Electronic Engineering, City University of Hong Kong, Kowloon, Hong Kong, China (e-mail: proton198601@hotmail.com).

L. Huang is with the Department of Electronic and Information Engineering, Harbin Institute of Technology Shenzhen Graduate School, Shenzhen 518055, China (e-mail: lhuang8sasp@hotmail.com).

Color versions of one or more of the figures in this paper are available online at http://ieeexplore.ieee.org.

Digital Object Identifier 10.1109/TSP.2013.2259163

II. Notation and Problem Formulation

A. Notation

Scalars, vectors, matrices and tensors are denoted by italic, bold lower-case, bold upper-case and bold calligraphic symbols, respectively. The angle and magnitude of a complex number a are written as $\angle(a)$ and $|a|$, while the variable, noise-free value and estimate of $\mathbf{A}$ are denoted by $\breve{\mathbf{A}}$, $\widetilde{\mathbf{A}}$ and $\widehat{\mathbf{A}}$. We use ^{T}, ^{H}, *, $^{-1}$ and † to represent the transpose, conjugate transpose, complex conjugate, inverse, and pseudoinverse of a vector or a matrix, and $\mathbf{I}_i$, $\mathbf{0}_{i\times j}$ and Π_i symbolize the $i\times i$ identity matrix, $i\times j$ zero matrix and $i\times i$ matrix with ones in its anti-diagonal and zeros elsewhere, respectively. The $\mathrm{diag}(\mathbf{a})$ denotes a diagonal matrix with vector $\mathbf{a}$ as the main diagonal. A R-D tensor whose $(f,f,\cdots,f)$ entry equals 1 and zero otherwise is defined as $\boldsymbol{\mathcal{I}}_F^R\in\mathbb{C}^{F\times F\times\cdots\times F}$. Furthermore, we write $\mathbf{A}:=\mathbf{B}$ to define $\mathbf{A}$ as $\mathbf{B}$ while vec is the vectorization operator, $\otimes$ represents the Kronecker product and $\mathbb{E}$ is the expectation operator. To refer to the ith element of $\mathbf{a}$, (i,j) entry of $\mathbf{A}$ and $(m_1,m_2,\ldots,m_R)$ entry of a R-D tensor $\boldsymbol{\mathcal{A}}\in\mathbb{C}^{M_1\times M_2\times\ldots\times M_R}$, we use $[\mathbf{a}]_i$, $[\mathbf{A}]_{i,j}$ and $a_{m_1,m_2,\ldots,m_R}$, respectively.

Regarding tensor operations, the rth unfolding of $\boldsymbol{\mathcal{A}}$ is written as $[\boldsymbol{\mathcal{A}}]_{(r)}\in\mathbb{C}^{M_r\times(M_1M_2\cdots M_{r-1}M_{r+1}\cdots M_R)}$ where the order of the columns is chosen according to [9]. Vectorization of $\boldsymbol{\mathcal{A}}$ is defined as $\mathrm{vec}(\boldsymbol{\mathcal{A}}):=\mathrm{vec}([\boldsymbol{\mathcal{A}}]_R^T)$. The r-mode product of tensor $\boldsymbol{\mathcal{A}}\in\mathbb{C}^{M_1\times M_2\times\ldots\times M_R}$ and matrix $\mathbf{U}\in\mathbb{C}^{N_r\times M_r}$ along the rth dimension is expressed as $\boldsymbol{\mathcal{B}}=\boldsymbol{\mathcal{A}}\times_r\mathbf{U}\in\mathbb{C}^{M_1\times M_2\times\cdots\times M_{r-1}\times N_r\times M_{r+1}\times\ldots\times M_R}$ where $[\boldsymbol{\mathcal{B}}]_{(r)}=\mathbf{U}[\boldsymbol{\mathcal{A}}]_{(r)}$. Note that $\boldsymbol{\mathcal{B}}$ can be interpreted as multiplying all r-mode vectors of $\boldsymbol{\mathcal{A}}$ by $\mathbf{U}$. The outer product of two tensors $\boldsymbol{\mathcal{A}}\in\mathbb{C}^{M_1\times M_2\times\ldots\times M_P}$ and $\boldsymbol{\mathcal{B}}\in\mathbb{C}^{N_1\times N_2\times\ldots\times N_Q}$ is a $(P+Q)$-D tensor of the form $\boldsymbol{\mathcal{C}}=\boldsymbol{\mathcal{A}}\circ\boldsymbol{\mathcal{B}}\in\mathbb{C}^{M_1\times M_2\times\ldots\times M_P\times N_1\times N_2\times\ldots\times N_Q}$ where $c_{m_1,m_2,\ldots,m_R,n_1,n_2,\ldots,n_R}=a_{m_1,m_2,\ldots,m_R}\cdot b_{n_1,n_2,\ldots,n_R}$ and $\circ$ is the outer product operator. The symbol $\sqcup$ represents the concatenation operator where $\boldsymbol{\mathcal{A}}=\boldsymbol{\mathcal{A}}_1\sqcup_r\boldsymbol{\mathcal{A}}_2$ is obtained by stacking $\boldsymbol{\mathcal{A}}_2\in\mathbb{C}^{M_1\times M_2\times\cdots\times M_{r-1}\times L_2\times M_{r+1}\times\cdots\times M_R}$ to the end of $\boldsymbol{\mathcal{A}}_1\in\mathbb{C}^{M_1\times M_2\times\cdots\times M_{r-1}\times L_1\times M_{r+1}\times\cdots\times M_R}$ along the rth dimension.

B. Problem Formulation

We consider the problem of R-D HR with multiple snapshots in the presence of additive noise. The noise-free tensor $\boldsymbol{\mathcal{X}}\in\mathbb{C}^{M_1\times M_2\times\ldots\times M_R\times N}$ has entries of the form:

$$x_{m_1,m_2,\ldots,m_R,n}=\sum_{f=1}^{F}\gamma_f(n)\prod_{r=1}^{R}e^{j\omega_{r,f}m_r} \tag{1}$$

where $n=1,2,\ldots,N$, $m_r=1,2,\ldots,M_r$, $r=1,2,\ldots,R$ and $f=1,2,\ldots,F$. The F, R and N are the number of frequencies, dimensions and snapshots, respectively. That is, together with the snapshots, the signal dimension is $(R+1)$. Along the rth dimension, the data length is M_r. The $\gamma_f(n)$ denotes the unknown complex amplitude of the fth tone at the nth snapshot with power $\mathbb{E}\{|\gamma_f(n)|^2\}=\sigma_f^2$ while $\omega_{r,f}\in(-\pi,\pi)$, $r=1,2,\ldots,R$, $f=1,2,\ldots,F$, are the R-D frequencies. The observed signal, denoted by $\boldsymbol{\mathcal{Y}}\in\mathbb{C}^{M_1\times M_2\times\ldots\times M_R\times N}$, is:

$$\boldsymbol{\mathcal{Y}}=\boldsymbol{\mathcal{X}}+\boldsymbol{\mathcal{Q}} \tag{2}$$

where $\boldsymbol{\mathcal{Q}}$ is the noise component and its entries are uncorrelated zero-mean circularly symmetric complex Gaussian (ZMCSCG) random variables with unknown but identical variance σ^2. Defining $M=\prod_{r=1}^{R}M_r$, we assume that $F\le\min\{M,N\}$. Note that when this condition is not satisfied, we can apply standard preprocessing schemes [15], [16], namely, forward-backward averaging and/or spatial smoothing, to virtually increase the number of available snapshots. Moreover, our proposed approach can be straightforwardly adapted for the more general damped sinusoidal model if forward-backward averaging is not employed. The task of R-D HR is to find $\{\omega_{r,f}\}$ from the observed tensor $\boldsymbol{\mathcal{Y}}$.

III. Proposed Estimator

According to the structure of (1), $\boldsymbol{\mathcal{X}}$ can be expressed as

$$\boldsymbol{\mathcal{X}}=\boldsymbol{\mathcal{I}}_F^{R+1}\times_1\mathbf{G}_1\times_2\mathbf{G}_2\cdots\times_R\mathbf{G}_R\times_{R+1}\mathbf{G}_{R+1} \tag{3}$$

where

$$\mathbf{G}_r=[\mathbf{g}_{r,1}\quad\mathbf{g}_{r,2}\quad\cdots\quad\mathbf{g}_{r,F}] \tag{4}$$

$$\mathbf{g}_{r,f}=[e^{j\omega_{r,f}}\quad e^{j2\omega_{r,f}}\quad\cdots\quad e^{jM_r\omega_{r,f}}]^T \tag{5}$$

$$\mathbf{g}_{R+1,f}=[\gamma_f(1)\quad\gamma_f(2)\quad\cdots\quad\gamma_f(N)]^T \tag{6}$$

with $r=1,2,\cdots,R$.

On the other hand, the HOSVD of $\boldsymbol{\mathcal{Y}}$ can be written as the following product [9]:

$$\boldsymbol{\mathcal{Y}}=\boldsymbol{\mathcal{S}}\times_1\mathbf{U}_1\times_2\mathbf{U}_2\cdots\times_R\mathbf{U}_R\times_{R+1}\mathbf{U}_{R+1} \tag{7}$$

where $\boldsymbol{\mathcal{S}}\in\mathbb{C}^{M_1\times M_2\times\ldots\times M_R\times N}$ is the core ordered tensor satisfying the property of all-orthogonality while $\mathbf{U}_r\in\mathbb{C}^{M_r\times M_r}$, $r=1,2,\cdots,R$, and $\mathbf{U}_{R+1}\in\mathbb{C}^{N\times N}$ are unitary matrices.

As $\boldsymbol{\mathcal{X}}$ is of rank F, it can be estimated by using the truncated HOSVD of $\boldsymbol{\mathcal{Y}}$ [9]:

$$\widehat{\boldsymbol{\mathcal{X}}}=\boldsymbol{\mathcal{S}}^{[s]}\times_1\mathbf{U}_1^{[s]}\times_2\mathbf{U}_2^{[s]}\cdots\times_R\mathbf{U}_R^{[s]}\times_{R+1}\mathbf{U}_{R+1}^{[s]} \tag{8}$$

where $\boldsymbol{\mathcal{S}}^{[s]}$ has only the first l_r elements of $\boldsymbol{\mathcal{S}}$ in the rth dimension and $\mathbf{U}_r^{[s]}\in\mathbb{C}^{M_r\times l_r}$ contains the first l_r dominant singular vectors of $\mathbf{U}_r$, with $l_r=\min\{F,M_r,MN/M_r\}$, $r=1,2,\cdots,R$, and $l_{R+1}=\min\{F,M\}$. Notice that we can also use the iterative approach in [10] to obtain the best rank-$(l_1,l_2,\cdots,l_{R+1})$ approximation of the tensor $\boldsymbol{\mathcal{Y}}$ but a much higher computational cost is required.

Based on (3) and (8), we define

$$\boldsymbol{\mathcal{G}}^{[s]}=\boldsymbol{\mathcal{I}}_F^{R+1}\times_1\mathbf{G}_1\times_2\mathbf{G}_2\cdots\times_R\mathbf{G}_R\in\mathbb{C}^{M_1\times M_2\times\ldots\times M_R\times F} \tag{9}$$

and

$$\boldsymbol{\mathcal{U}}^{[s]} = \boldsymbol{\mathcal{S}}^{[s]} \times_1 \mathbf{U}_1^{[s]} \times_2 \mathbf{U}_2^{[s]} \cdots \times_R \mathbf{U}_R^{[s]} \in \mathbb{C}^{M_1 \times M_2 \times \ldots \times M_R \times F} \tag{10}$$

Note that $\boldsymbol{\mathcal{U}}^{[s]}$ corresponds to the tensor-based signal subspace [15]. Comparing with the standard matrix-based processing [14]–[18], SVD truncation is performed on $[\boldsymbol{\mathcal{Y}}]_{(R+1)}^T$ to obtain the signal subspace $\mathbf{U}_s \in \mathbb{C}^{M \times F}$:

$$[\boldsymbol{\mathcal{Y}}]_{(R+1)}^T = \mathbf{U}\mathbf{S}\mathbf{V}^H = \mathbf{U}_s\mathbf{S}_s\mathbf{V}_s^H + \mathbf{U}_n\mathbf{S}_n\mathbf{V}_n^H \tag{11}$$

According to [15] and [21], the columns of $[\boldsymbol{\mathcal{U}}^{[s]}]_{(R+1)}^T$ span exactly the same subspace as $\mathbf{U}_s$ when $F \geq \max\{M_1, M_2, \cdots, M_R\}$. However, since $[\boldsymbol{\mathcal{U}}^{[s]}]_{(R+1)}^T$ is computed from HOSVD which utilizes the tensor structure while SVD cannot, and its noise components are more well-structured and/or less than those of $\mathbf{U}_s$ when $F < \max\{M_1, M_2, \cdots, M_R\}$. In this work, we devise an eigenvector-based approach by exploiting the tensorial structure of $\boldsymbol{\mathcal{U}}^{[s]}$, which is referred to as tensor-eigenvector (TEV) estimator.

From [18], we know that when $F \leq \min\{M, N\}$, $[\boldsymbol{\mathcal{G}}^{[s]}]_{(R+1)}^T$ has full column rank almost surely, and $[\boldsymbol{\mathcal{U}}^{[s]}]_{(R+1)}^T$ has F columns that together span the same column space of $[\boldsymbol{\mathcal{X}}]_{(R+1)}^T$, which is also spanned by $[\boldsymbol{\mathcal{G}}^{[s]}]_{(R+1)}^T$. Hence, under sufficiently small noise conditions, there exists an $F \times F$ nonsingular matrix $\mathbf{T}$ such that

$$\left[\boldsymbol{\mathcal{U}}^{[s]}\right]_{(R+1)} \approx \mathbf{T}\left[\boldsymbol{\mathcal{G}}^{[s]}\right]_{(R+1)} \tag{12}$$

Equation (12) can be written in tensor form as:

$$\boldsymbol{\mathcal{U}}^{[s]} \approx \boldsymbol{\mathcal{G}}^{[s]} \times_{R+1} \mathbf{T}^T \tag{13}$$

Similar to [17], [18], we construct $(R+1)$ sub-tensors $\boldsymbol{\mathcal{U}}_{s1}^{[s]}$ and $\boldsymbol{\mathcal{U}}_r^{[s]}$, $r = 1, 2, \cdots, R$:

$$\begin{aligned}\boldsymbol{\mathcal{U}}_{s1}^{[s]} &= \boldsymbol{\mathcal{U}}^{[s]} \times_1 \mathbf{J}_{1,1} \times_2 \mathbf{J}_{1,2} \cdots \times_R \mathbf{J}_{1,R} \\ &= \boldsymbol{\mathcal{S}}^{[s]} \times_1 \mathbf{J}_{1,1}\mathbf{U}_1^{[s]} \times_2 \mathbf{J}_{1,2}\mathbf{U}_2^{[s]} \cdots \times_R \mathbf{J}_{1,R}\mathbf{U}_R^{[s]} \qquad (14) \\ \boldsymbol{\mathcal{U}}_r^{[s]} &= \boldsymbol{\mathcal{S}}^{[s]} \times_1 \mathbf{J}_{1,1}\mathbf{U}_1^{[s]} \cdots \times_{r-1} \mathbf{J}_{1,r-1}\mathbf{U}_{r-1}^{[s]} \times_r \mathbf{J}_{2,r}\mathbf{U}_r^{[s]} \\ &\quad \times_{r+1} \mathbf{J}_{1,r+1}\mathbf{U}_{r+1}^{[s]} \cdots \times_R \mathbf{J}_{1,R}\mathbf{U}_R^{[s]} \qquad (15)\end{aligned}$$

where

$$\mathbf{J}_{1,r} = [\mathbf{I}_{M_r-1} \quad \mathbf{0}_{(M_r-1)\times 1}] \tag{16}$$

$$\mathbf{J}_{2,r} = [\mathbf{0}_{(M_r-1)\times 1} \quad \mathbf{I}_{M_r-1}] \tag{17}$$

are selection matrices. In the absence of noise, we have:

$$\widetilde{\boldsymbol{\mathcal{U}}}_{s1}^{[s]} \times_{R+1} \widetilde{\boldsymbol{\Psi}}_r^T = \widetilde{\boldsymbol{\mathcal{U}}}_r^{[s]} \tag{18}$$

where

$$\widetilde{\boldsymbol{\Psi}}_r = \widetilde{\mathbf{T}}_r\boldsymbol{\Phi}_r\widetilde{\mathbf{T}}_r^{-1} \tag{19}$$

with $\widetilde{\mathbf{T}}_r$ being a nonsingular matrix and $\boldsymbol{\Phi}_r$ is a diagonal matrix which contains the frequency information:

$$\boldsymbol{\Phi}_r = \operatorname{diag}\left([e^{j\omega_{r,1}} \quad e^{j\omega_{r,2}} \quad \cdots \quad e^{j\omega_{r,F}}]\right) \tag{20}$$

In the practical scenario where noise is present, the equality of (18) approximately holds, meaning that

$$\boldsymbol{\mathcal{U}}_{s1}^{[s]} \times_{R+1} \mathbf{T}_r^T\boldsymbol{\Phi}_r \approx \boldsymbol{\mathcal{U}}_r^{[s]} \times_{R+1} \mathbf{T}_r^T \tag{21}$$

because $\boldsymbol{\Phi}_r = \boldsymbol{\Phi}_r^T$.

Employing (13), the estimate of $\boldsymbol{\mathcal{G}}^{[s]}$ can be solved as

$$\widehat{\boldsymbol{\mathcal{G}}}^{[s]} \approx \boldsymbol{\mathcal{U}}^{[s]} \times_{R+1} \mathbf{T}_r^T \tag{22}$$

from which the frequencies can be determined.

However, when there are identical frequencies in (20), (22) fails to give reliable estimation of $\boldsymbol{\mathcal{G}}^{[s]}$ [17]. To overcome this limitation, we follow [18] to construct

$$\boldsymbol{\mathcal{U}}_{s2}^{[s]} = \sum_{r=1}^{R} \alpha_r \boldsymbol{\mathcal{U}}_r^{[s]} \tag{23}$$

where $\{\alpha_r\}_{r=1}^R$ are a set of complex weighting factors. Analogous to (18), we obtain:

$$\boldsymbol{\mathcal{U}}_{s1}^{[s]} \times_{R+1} \boldsymbol{\Psi}_s^T \approx \boldsymbol{\mathcal{U}}_{s2}^{[s]} \tag{24}$$

where

$$\boldsymbol{\Psi}_s = \mathbf{T}_s\boldsymbol{\Phi}_s\mathbf{T}_s^{-1} \tag{25}$$

with $\mathbf{T}_s$ being a nonsingular matrix and

$$\begin{aligned}\boldsymbol{\Phi}_s &= \operatorname{diag}\left([\phi_1 \quad \phi_2 \quad \cdots \quad \phi_F]\right) \\ \phi_f &= \sum_{r=1}^{R} \alpha_r e^{j\omega_{r,f}}\end{aligned} \tag{26}$$

When $\{\alpha_r\}_{r=1}^R$ are properly chosen, $\phi_i \neq \phi_j$ for $i \neq j$ can be obtained even in the presence of identical frequencies in one or more dimensions. According to [18] an optimal vector of $\boldsymbol{\alpha} = [\alpha_1 \ \alpha_2 \ \cdots \ \alpha_R]^T$ can be computed from:

$$\begin{aligned}\boldsymbol{\alpha} &= \arg\min_{\breve{\boldsymbol{\alpha}}} \sum_{i=1}^{F-1} \sum_{j=i+1}^{F} \frac{1}{\left\|\left(\boldsymbol{\rho}_i^T - \boldsymbol{\rho}_j^T\right)\breve{\boldsymbol{\alpha}}\right\|_2^2} \\ \text{subject to } \boldsymbol{\rho}_i &= [e^{j\omega_{1,i}} \ e^{j\omega_{2,i}} \ \cdots \ e^{j\omega_{R,i}}]^T \\ &\|\breve{\boldsymbol{\alpha}}\|_2 \leq 1\end{aligned} \tag{27}$$

The main idea of (27) is to minimize the mean square frequency error of the estimator. Note that the constraint of $\|\breve{\boldsymbol{\alpha}}\|_2 \leq 1$ is to avoid the solution of infinite values of $\{\alpha_r\}$. In our study, minimizing the sum of the inverse of $\|(\boldsymbol{\rho}_i^T - \boldsymbol{\rho}_j^T)\breve{\boldsymbol{\alpha}}\|_2^2$ in (27) is approximated by the maximization of the sum of $\|(\boldsymbol{\rho}_i^T - \boldsymbol{\rho}_j^T)\breve{\boldsymbol{\alpha}}\|_2^2$. Moreover, the inequality constraint is modified to $\|\breve{\boldsymbol{\alpha}}\|_2 \leq 1$. That is, we propose to approximate (27) as:

$$\begin{aligned}\boldsymbol{\alpha} &= \arg\max_{\breve{\boldsymbol{\alpha}}} f(\breve{\boldsymbol{\alpha}}) \\ \text{subject to} \quad &\|\breve{\boldsymbol{\alpha}}\|_2 = 1\end{aligned} \tag{28}$$

where

$$f(\breve{\boldsymbol{\alpha}}) = \sum_{i=1}^{F-1} \sum_{j=i+1}^{F} \left\| \left(\boldsymbol{\rho}_i^T - \boldsymbol{\rho}_j^T\right) \breve{\boldsymbol{\alpha}} \right\|_2^2 = \breve{\boldsymbol{\alpha}}^H \boldsymbol{\Omega}^H \boldsymbol{\Omega} \breve{\boldsymbol{\alpha}} \tag{29}$$

with

$$\begin{aligned} \boldsymbol{\Omega} &= [\boldsymbol{\rho}_{1,2}\ \boldsymbol{\rho}_{1,3}\ \cdots\ \boldsymbol{\rho}_{1,F}\ \boldsymbol{\rho}_{2,3}\ \cdots\ \boldsymbol{\rho}_{F-1,F}]^T \\ &\quad \in \mathbb{C}^{F(F-1)\times R} \\ \boldsymbol{\rho}_{i,j} &= \boldsymbol{\rho}_i - \boldsymbol{\rho}_j \end{aligned} \tag{30}$$

It is easy to show that the solution of (28) can be given by the eigenvector corresponding to the largest eigenvalue of $\boldsymbol{\Omega}^H\boldsymbol{\Omega}$. As $\boldsymbol{\Omega}$ is a function of the unknown frequencies, iterative estimation of $\{\omega_{r,f}\}$ and $\boldsymbol{\alpha}$ is thus required. It is worth pointing out the solution of (28) can be employed as an initial guess for solving (27) with a numerical technique such as Newton-Raphson or steepest descent method. However, we have found that there is no obvious improvement in estimation accuracy and much higher computational load is required, and thus their results are not included.

Now we present the frequency estimation procedure for a given $\boldsymbol{\alpha}$ that satisfies $\phi_i \neq \phi_j$ for $i \neq j$ in (26) and then summarize the complete algorithm.Similar to (21), (24) implies

$$\boldsymbol{\mathcal{U}}_{s1}^{[s]} \times_{R+1} \mathbf{T}_s^T \boldsymbol{\Phi}_s \approx \boldsymbol{\mathcal{U}}_{s2}^{[s]} \times_{R+1} \mathbf{T}_s^T \tag{31}$$

The modified estimate of $\boldsymbol{\mathcal{G}}^{[s]}$ is then:

$$\begin{aligned} \widehat{\boldsymbol{\mathcal{G}}}^{[s]} &\approx \boldsymbol{\mathcal{U}}^{[s]} \times_{R+1} \mathbf{T}_s^T \\ &= \mathbf{Z}_1 \sqcup_{R+1} \mathbf{Z}_2 \sqcup_{R+1} \cdots \sqcup_{R+1} \mathbf{Z}_F \end{aligned} \tag{32}$$

where

$$\mathbf{Z}_f \approx \beta_f \mathbf{g}_{1,f} \circ \mathbf{g}_{2,f} \cdots \circ \mathbf{g}_{R,f}, \quad f = 1, 2, \cdots, F \tag{33}$$

with $\{\beta_f\}$ being unknown complex scalars. That is, (32) provides F sub-tensors and each of them contains only one tone. Applying the truncated HOSVD to each $\boldsymbol{\mathcal{Z}}_f$ yields

$$\boldsymbol{\mathcal{Z}}_f \approx \lambda_f \times_1 \mathbf{h}_{1,f} \times_2 \mathbf{h}_{2,f} \cdots \times_R \mathbf{h}_{R,f} \tag{34}$$

where

$$[\boldsymbol{\mathcal{Z}}_f]_r \approx \mathbf{h}_{r,f} \lambda_{r,f} \mathbf{v}_{r,f} \tag{35}$$

is the rank-1 SVD truncation with $|\lambda_f|^2 = \lambda_{r,f}^2$ for any r [9]. Comparing (33) and (34) and according to [19], it is seen that the noise-free $\mathbf{h}_{r,f}$ spans the same subspace as $\mathbf{g}_{r,f}$, meaning that $\mathbf{h}_{r,f} \approx \beta_{r,f}\mathbf{g}_{r,f}$ where $\beta_{r,f}$ is a complex scalar. Together with the linear prediction property of $\mathbf{g}_{r,f}$, we obtain:

$$\mathbf{J}_{1,r}\mathbf{h}_{r,f}\rho_{r,f} \approx \mathbf{J}_{2,r}\mathbf{h}_{r,f}, \quad \rho_{r,f} = e^{j\omega_{r,f}} \tag{36}$$

which corresponds to a system of linear equations of $\{\rho_{r,f}\}$. To utilize the inherent structure in (36), SLS [13] is applied to solve for $\{\rho_{r,f}\}$ as follows.

Define

$$\mathbf{h}_{r,f}^{\mathrm{SLS}} = \mathbf{h}_{r,f} + \boldsymbol{\Delta}\mathbf{h}_{r,f}^{\mathrm{SLS}} \tag{37}$$

as the SLS estimate of $\mathbf{h}_{r,f}$, which is a basis vector of the improved signal subspace estimate. The $\mathbf{h}_{r,f}^{\mathrm{SLS}}$ can be determined such that the norm of the residual vector $\mathbf{R}(\rho_{r,f}, \mathbf{h}_{r,f}^{\mathrm{SLS}}) = \mathbf{J}_{1,r}\mathbf{h}_{r,f}^{\mathrm{SLS}}\rho_{r,f} - \mathbf{J}_{2,r}\mathbf{h}_{r,f}^{\mathrm{SLS}}$ is minimized. Given $\mathbf{h}_{r,f}$ from (34), the updated SLS estimates of $\rho_{r,f}$ and $\boldsymbol{\Delta}\mathbf{h}_{r,f}^{\mathrm{SLS}}$ are determined from

$$\min_{\rho_{r,f}, \boldsymbol{\Delta}\mathbf{h}_{r,f}^{\mathrm{SLS}}} \left\| \begin{bmatrix} \mathbf{R}\left(\rho_{r,f}, \mathbf{h}_{r,f}^{\mathrm{SLS}}\right) \\ \kappa_r \boldsymbol{\Delta}\mathbf{h}_{r,f}^{\mathrm{SLS}} \end{bmatrix} \right\|_2 \tag{38}$$

where κ_r is a weighting factor that provides a normalization between the two vectors in (38) and is chosen in accordance with [13]. The minimization problem of (38) is solved in an iterative manner. We define $\mathbf{R}(\rho_{r,f}|_k, \mathbf{h}_{r,f}^{\mathrm{SLS}}|_k) = \mathbf{J}_{1,r}\mathbf{h}_{r,f}^{\mathrm{SLS}}|_k\rho_{r,f}|_k - \mathbf{J}_{2,r}\mathbf{h}_{r,f}^{\mathrm{SLS}}|_k$ as the residual vector at the kth iteration where $k \geq 0$, and let

$$\boldsymbol{\Delta}\mathbf{h}_{r,f,k}^{\mathrm{SLS}} = \sum_{j=0}^{k-1} \boldsymbol{\Delta}\mathbf{h}_{r,f}^{\mathrm{SLS}}|_j \tag{39}$$

be the total subspace change at the kth iteration step such that

$$\mathbf{h}_{r,f}^{\mathrm{SLS}}|_k = \mathbf{h}_{r,f} + \boldsymbol{\Delta}\mathbf{h}_{r,f,k}^{\mathrm{SLS}} \tag{40}$$

At the $(k+1)$th iteration, we have

$$\begin{aligned} &\mathbf{R}\left(\rho_{r,f}|_{k+1}, \mathbf{h}_{r,f}^{\mathrm{SLS}}|_{k+1}\right) \\ &\quad = \mathbf{R}\left(\rho_{r,f}|_k + \boldsymbol{\Delta}\rho_{r,f}|_k, \mathbf{h}_{r,f}^{\mathrm{SLS}}|_k + \boldsymbol{\Delta}\mathbf{h}_{r,f}^{\mathrm{SLS}}|_k\right) \\ &\quad = \mathbf{J}_{1,r}\left(\mathbf{h}_{r,f}^{\mathrm{SLS}}|_k + \boldsymbol{\Delta}\mathbf{h}_{r,f}^{\mathrm{SLS}}|_k\right)\left(\rho_{r,f}|_k + \boldsymbol{\Delta}\rho_{r,f}|_k\right) \\ &\qquad - \mathbf{J}_{2,r}\left(\mathbf{h}_{r,f}^{\mathrm{SLS}}|_k + \boldsymbol{\Delta}\mathbf{h}_{r,f}^{\mathrm{SLS}}|_k\right) \\ &\quad \approx \mathbf{R}\left(\rho_{r,f}|_k, \mathbf{h}_{r,f}^{\mathrm{SLS}}|_k\right) \\ &\qquad + \mathbf{J}_{1,r}\left(\mathbf{h}_{r,f}^{\mathrm{SLS}}|_k\boldsymbol{\Delta}\rho_{r,f}|_k + \boldsymbol{\Delta}\mathbf{h}_{r,f}^{\mathrm{SLS}}|_k\rho_{r,f}|_k\right) \\ &\qquad - \mathbf{J}_{2,r}\boldsymbol{\Delta}\mathbf{h}_{r,f}^{\mathrm{SLS}}|_k \end{aligned} \tag{41}$$

Ignoring the second-order term of $\mathbf{J}_{1,r}\boldsymbol{\Delta}\mathbf{h}_{r,f}^{\mathrm{SLS}}|_k\boldsymbol{\Delta}\rho_{r,f}|_k$, (38) can be linearized as

$$\min_{\boldsymbol{\Delta}\rho_{r,f}|_k, \boldsymbol{\Delta}\mathbf{h}_{r,f}^{\mathrm{SLS}}|_k} \left\| \mathbf{B} \begin{bmatrix} \boldsymbol{\Delta}\rho_{r,f}|_k \\ \boldsymbol{\Delta}\mathbf{h}_{r,f}^{\mathrm{SLS}}|_k \end{bmatrix} + \begin{bmatrix} \mathbf{R}\left(\rho_{r,f}|_k, \mathbf{h}_{r,f}^{\mathrm{SLS}}|_k\right) \\ \kappa_r \boldsymbol{\Delta}\mathbf{h}_{r,f,k}^{\mathrm{SLS}} \end{bmatrix} \right\|_2 \tag{42}$$

where

$$\mathbf{B} = \begin{bmatrix} \mathbf{J}_{1,r}\boldsymbol{\Delta}\mathbf{h}_{r,f,k}^{\mathrm{SLS}} & \rho_{r,f}|_k\mathbf{J}_{1,r} - \mathbf{J}_{2,r} \\ \mathbf{0}_{(M_r-1)\times 1} & \kappa_r\mathbf{I}_{M_r-1} \end{bmatrix}$$

Using $\mathbf{h}_{r,f}^{\mathrm{SLS}}|_0 = \mathbf{h}_{r,f}$ from (34) and $\rho_{r,f}|_0 = (\mathbf{J}_{1,r}\mathbf{h}_{r,f})^{\dagger}\mathbf{J}_{2,r}\mathbf{h}_{r,f}$ from (36) as the initial estimates, $\boldsymbol{\Delta}\rho_{r,f}|_k$ and $\boldsymbol{\Delta}\mathbf{h}_{r,f}^{\mathrm{SLS}}|_k$ are computed as

$$\begin{bmatrix} \boldsymbol{\Delta}\rho_{r,f}|_k \\ \boldsymbol{\Delta}\mathbf{h}_{r,f}^{\mathrm{SLS}}|_k \end{bmatrix} = -\mathbf{B}^{\dagger} \begin{bmatrix} \mathbf{R}\left(\rho_{r,f}|_k, \mathbf{h}_{r,f}^{\mathrm{SLS}}|_k\right) \\ \kappa_r \boldsymbol{\Delta}\mathbf{h}_{r,f,k}^{\mathrm{SLS}} \end{bmatrix} \tag{43}$$

and $\rho_{r,f}|_{k+1} = \rho_{r,f}|_k + \Delta\rho_{r,f}|_k$, $\boldsymbol{\Delta}\mathbf{h}_{r,f,k}^{\mathrm{SLS}}$ and $\mathbf{h}_{r,f}^{\mathrm{SLS}}|_k$ are updated at each iteration.

TABLE I
TEV ESTIMATION ALGORITHM

(i) Compute HOSVD of $\mathcal{Y}$ to obtain $\mathcal{U}^{[s]}$ in (10), and generate random $\boldsymbol{\alpha}$ with each element $|\alpha_r| = 1/\sqrt{R}$
for $l = 1, 2, \cdots, \iota_2$, **do**
(ii) Construct $\mathcal{U}_{s1}^{[s]}$ and $\mathcal{U}_{s2}^{[s]}$ according to (14) and (23), then compute $\boldsymbol{\Psi}_s = ([\mathcal{U}_{s1}^{[s]}]_{R+1}^T)^\dagger [\mathcal{U}_{s2}^{[s]}]_{R+1}^T$ from (24)
(iii) Perform EVD on $\boldsymbol{\Psi}_s$ to obtain $\mathbf{T}_s$ of (25) and solve $\widehat{\mathcal{G}}$ according to (32) as $[\widehat{\mathcal{G}}]_{R+1}^T = [\mathcal{U}^{[s]}]_{R+1}^T \mathbf{T}_s$
(iv) For each f, $f = 1, 2, \cdots, F$, extract $\boldsymbol{\mathcal{Z}}_f$ from $\widehat{\mathcal{G}}$ and perform truncated HOSVD to obtain $\mathbf{h}_{r,f}$, $r = 1, 2, \cdots, R$
(v) For every $\mathbf{h}_{r,f}$, compute the LS solution $\rho_{r,f}|_0$ based on (36).
(vi) **if** $l = \iota_2$, **do**
for $k = 1, 2, \cdots, \iota_1$, solve $\boldsymbol{\Delta}\rho_{r,f}|_k$ and $\boldsymbol{\Delta}\mathbf{h}_{r,f}^{\mathrm{SLS}}|_k$ using (43) and update $\rho_{r,f}|_{k+1}$, $\boldsymbol{\Delta}\mathbf{h}_{r,f,k}^{\mathrm{SLS}}$ and $\mathbf{h}_{r,f}^{\mathrm{SLS}}|_k$
end if
(vii) Determine $\hat{\omega}_{r,f}$, $r = 1, 2, \cdots, R$, $f = 1, 2, \cdots, F$, based on (44). Note that the frequencies are all paired up
(viii) Construct $\boldsymbol{\Omega}$ according to (30) and compute dominant eigenvector of $\boldsymbol{\Omega}^H\boldsymbol{\Omega}$ to get updated $\boldsymbol{\alpha}$
end for

Employing ι_1 iterations as the stopping criterion, the frequency estimate is then:

$$\hat{\omega}_{r,f} = \angle\hat{\rho}_{r,f} = \angle\rho_{r,f}|_{\iota_1} \tag{44}$$

Note that when $\iota_1 = 0$, it is reduced to the standard least squares (LS) solution. In our simulation study, it is shown that $\iota_1 = 1$ is sufficient to provide accurate estimation.

Starting with $\{\alpha_r\}$ whose phases are uniformly chosen between $[-\pi, \pi)$ with $|\alpha_r| = \sqrt{1/R}$, the complete frequency estimation procedure is summarized in Table I. That is, ι_2 iterations are used to update $\boldsymbol{\alpha}$ while we compute the SLS solution only once when $\boldsymbol{\alpha}$ is finalized. Note also that the matrix operations for (24) and (32) are provided.

The major computational complexity of the TEV algorithm is studied as follows. First, the HOSVD of $\mathcal{Y}$ involves $(R+1)$ SVDs, which is of $\mathcal{O}(k_t F(R+1)\prod_{r=1}^R M_r N) = \mathcal{O}(k_t F(R+1)MN)$, where k_t is a constant depending on the design of the algorithm [22]. This step is most computationally demanding but only needs to compute once. Second, the complexity for the truncated HOSVD of F sub-tensors $\boldsymbol{\mathcal{Z}}_f \in \mathbb{C}^{M_1 \times M_2 \times \cdots \times M_R}$, $f = 1, 2, \cdots, F$, with ι_2 times, is $\mathcal{O}(k_t F M \iota_2)$ because $\boldsymbol{\mathcal{Z}}_f$ contains only one frequency. Finally, the SLS update of (43) requires a pseudoinverse whose complexity is $\mathcal{O}(F\iota_1 \sum_{r=1}^R M_r^3)$. Combining the results, the overall computational requirement is $\mathcal{O}(k_t F(R+1)MN) + \mathcal{O}(k_t F M \iota_2) + \mathcal{O}(F\iota_1 \sum_{r=1}^R M_r^3)$. In order to achieve a higher estimation accuracy, we can substitute $\mathcal{Y}$ with its forward-backward (FB) averaging version, denoted by $\mathcal{Y}^{(\mathrm{FB})}$:

$$\mathcal{Y}^{(\mathrm{FB})} = \mathcal{Y} \sqcup_{R+1} \mathcal{Y}^* \times \Pi_{M_1} \times \Pi_{M_2} \times \cdots \times \Pi_N \tag{45}$$

in Table I. Although the tensor size is larger, the main complexity order remains unchanged while N will be replaced by $2N$.

Finally, the identifiability of the TEV method is analyzed. Here, we assume that the observed tensor is modified via FB averaging of (45) and spatial smoothing [15] as $\mathcal{Y}' \in \mathbb{C}^{L_1 \times L_2 \times \cdots \times L_R \times N'}$ where $N' = 2N\prod_{r=1}^R K_r$ and $L_r + K_r - 1 = M_r$ for $r = 1, 2, \cdots, R$. In doing so, the maximum number of frequencies it can identify is $\min\{\prod_{r=1}^R (L_r - 1), N'\}$, which is identical to that of [18]. Since the results of using $\mathcal{U}^{[s]}$ in (10) and $\mathbf{U}_s$ in (11) are the same [15] when $F \geq \max\{L_1, L_2, \cdots, L_R\}$, we suggest to use the latter for efficient computation in this case.

IV. PERFORMANCE ANALYSIS

Making use of the perturbation analysis, the mean and variance of the proposed frequency estimator is derived in this section. We first assume that in the noise free case, the singular values of $\widetilde{\boldsymbol{\Psi}}_s = ([\widetilde{\mathcal{U}}_{s1}^{[s]}]_{R+1}^T)^\dagger [\widetilde{\mathcal{U}}_{s2}^{[s]}]_{R+1}^T$ in (26) are distinct, which are valid when an appropriate set of $\{\alpha_r\}_{r=1}^R$ is chosen. According to (8), the truncated HOSVD of $\boldsymbol{\mathcal{X}}$ is:

$$\boldsymbol{\mathcal{X}} = \widetilde{\boldsymbol{\mathcal{S}}}^{[s]} \times_1 \widetilde{\mathbf{U}}_1^{[s]} \times_2 \widetilde{\mathbf{U}}_2^{[s]} \cdots \times_R \widetilde{\mathbf{U}}_R^{[s]} \times_{R+1} \widetilde{\mathbf{U}}_{R+1}^{[s]} \tag{46}$$

where

$$[\boldsymbol{\mathcal{X}}]_r = \widetilde{\mathbf{U}}_r^{[s]} \widetilde{\boldsymbol{\Sigma}}_r^{[s]} \widetilde{\mathbf{V}}_r^{[s]^H} + \widetilde{\mathbf{U}}_r^{[n]} \widetilde{\boldsymbol{\Sigma}}_r^{[n]} \widetilde{\mathbf{V}}_r^{[n]^H}$$
$$r = 1, 2, \cdots, R+1 \tag{47}$$

with $\widetilde{\mathbf{U}}_r^{[n]}$, $\widetilde{\boldsymbol{\Sigma}}_r^{[n]}$ and $\widetilde{\mathbf{V}}_r^{[n]}$ being the noise subspace components.

In the presence of noise, we have $\boldsymbol{\mathcal{S}}^{[s]} = \widetilde{\boldsymbol{\mathcal{S}}}^{[s]} + \boldsymbol{\Delta}\boldsymbol{\mathcal{S}}^{[s]}$ and $\mathbf{U}_r^{[s]} = \widetilde{\mathbf{U}}_r^{[s]} + \boldsymbol{\Delta}\mathbf{U}_r^{[s]}$ where $\boldsymbol{\Delta}\mathbf{U}_r^{[s]}$ has the form [23]:

$$\boldsymbol{\Delta}\mathbf{U}_r^{[s]} = \widetilde{\mathbf{U}}_r^{[n]} \widetilde{\mathbf{U}}_r^{[n]^H} [\boldsymbol{\mathcal{Q}}]_r \widetilde{\mathbf{V}}_r^{[s]} \widetilde{\boldsymbol{\Sigma}}_r^{[s]^{-1}} \tag{48}$$

Comparing (47) and (11), we notice that the matrix-based signal subspace can be expressed as

$$\mathbf{U}_s = \mathbf{V}_{R+1}^{[s]^*} \tag{49}$$

To simplify the notation, we employ $\mathbf{U}_{s\mathrm{T}} := [\mathcal{U}^{[s]}]_{R+1}^T$ to represent the tensor-based signal subspace. According to [21], we have

$$\boldsymbol{\Delta}\mathbf{U}_{s\mathrm{T}} \approx (\widetilde{\Upsilon}_1 \otimes \widetilde{\Upsilon}_2 \otimes \cdots \otimes \widetilde{\Upsilon}_R)\boldsymbol{\Delta}\mathbf{U}_s \widetilde{\boldsymbol{\Sigma}}_{R+1}^{[s]} + \sum_{r=1}^R \widetilde{\mathbf{H}}_r \tag{50}$$

where

$$\widetilde{\mathbf{H}}_r = \Big(\widetilde{\Upsilon}_1 \otimes \cdots \otimes \widetilde{\Upsilon}_{r-1} \otimes (\boldsymbol{\Delta}\mathbf{U}_r^{[s]} \widetilde{\mathbf{U}}_r^{[s]^H}) \otimes \widetilde{\Upsilon}_{r+1} \otimes \cdots \otimes \widetilde{\Upsilon}_R\Big) \mathbf{U}_s \widetilde{\boldsymbol{\Sigma}}_{R+1}^{[s]} \tag{51}$$

with $\widetilde{\Upsilon}_r = \widetilde{\mathbf{U}}_r^{[s]} \widetilde{\mathbf{U}}_r^{[s]^H}$.

The perturbations of $\mathbf{U}_{s\mathrm{T}1} := [\mathcal{U}_{s1}^{[s]}]_{R+1}^T$ and $\mathbf{U}_{s\mathrm{T}2} := [\mathcal{U}_{s2}^{[s]}]_{R+1}^T$ are then

$$\boldsymbol{\Delta}\mathbf{U}_{s\mathrm{T}1} = \mathbf{J}_1 \boldsymbol{\Delta}\mathbf{U}_{s\mathrm{T}} \tag{52}$$

and

$$\boldsymbol{\Delta}\mathbf{U}_{s\mathrm{T}2} = \mathbf{J}_2 \boldsymbol{\Delta}\mathbf{U}_{s\mathrm{T}} \tag{53}$$

where $\mathbf{J}_1 = \mathbf{J}_{1,1} \otimes \mathbf{J}_{1,2} \otimes \cdots \otimes \mathbf{J}_{1,R}$ and $\mathbf{J}_2 = \sum_{r=1}^R \mathbf{J}_{2r}$, $\mathbf{J}_{2r} = \mathbf{J}_{1,1} \otimes \cdots \otimes \mathbf{J}_{1,r-1} \otimes \mathbf{J}_{2,r} \otimes \mathbf{J}_{1,r+1} \otimes \cdots \otimes \mathbf{J}_{1,R}$.

According to (24), we have $\mathbf{U}_{s\mathrm{T}1}\mathbf{T}_s\mathbf{\Phi}_s = \mathbf{U}_{s\mathrm{T}2}\mathbf{T}_s$. Let $\mathbf{T}_s = [\mathbf{t}_1\ \mathbf{t}_2\ \cdots\ \mathbf{t}_R]$, then we obtain:

$$(\widetilde{\mathbf{U}}_{s\mathrm{T}1} + \mathbf{\Delta U}_{s\mathrm{T}1})(\tilde{\mathbf{t}}_f + \mathbf{\Delta t}_f)(\tilde{\phi}_f + \Delta\phi_f) = (\widetilde{\mathbf{U}}_{s\mathrm{T}2} + \mathbf{\Delta U}_{s\mathrm{T}2})(\tilde{\mathbf{t}}_f + \mathbf{\Delta t}_f) \quad (54)$$

for $f = 1, 2, \cdots, F$. Ignoring the second-order terms, (54) becomes

$$(\mathbf{J}_1\tilde{\phi}_f - \mathbf{J}_2)\mathbf{\Delta U}_{s\mathrm{T}}\tilde{\mathbf{t}}_f + \mathbf{J}_1\widetilde{\mathbf{U}}_{s\mathrm{T}}\tilde{\mathbf{t}}_f\Delta\phi_f = -(\mathbf{J}_1\tilde{\phi}_f - \mathbf{J}_2)\widetilde{\mathbf{U}}_{s\mathrm{T}}\mathbf{\Delta t}_f \quad (55)$$

Following [18], $\mathbf{\Delta t}_f = \mathbf{D}_f\mathbf{\Delta U}_{s\mathrm{T}}\tilde{\mathbf{t}}_f$ is obtained where $\mathbf{D}_f$ is:

$$\mathbf{D}_f = -\widetilde{\mathbf{T}}_s\widetilde{\mathbf{\Xi}}_f\left(\left[\tilde{\boldsymbol{\mathcal{U}}}^{[s]}\right]_{R+1}^{T}\widetilde{\mathbf{T}}_s^T\right)^{\dagger}(\mathbf{J}_1\tilde{\phi}_f - \mathbf{J}_2) \quad (56)$$

Here, $\widetilde{\mathbf{\Xi}}_f$ is a diagonal matrix with $[\widetilde{\mathbf{\Xi}}_f]_{g,g} = 1/(\tilde{\phi}_f - \tilde{\phi}_g)$ for $g \neq f$, and $[\widetilde{\mathbf{\Xi}}_f]_{f,f} = 0$. Furthermore, since the transpose of the $(R+1)$th unfolding of the subtensor $\boldsymbol{\mathcal{Z}}_f$ is obtained using $\mathbf{z}_{f\mathrm{T}} := [\boldsymbol{\mathcal{Z}}_f]_{R+1}^{T} = \mathbf{U}_{s\mathrm{T}}\mathbf{t}_f$, we have

$$\begin{aligned}\mathbf{\Delta z}_{f\mathrm{T}} &= \mathbf{\Delta U}_{s\mathrm{T}}\mathbf{t}_f + \mathbf{U}_{s\mathrm{T}}\mathbf{\Delta t}_f = (\mathbf{I}_M + \widetilde{\mathbf{U}}_{s\mathrm{T}}\mathbf{D}_f)\mathbf{\Delta U}_{s\mathrm{T}}\tilde{\mathbf{t}}_f \\ &= \mathbf{r}_f\mathrm{vec}(\mathbf{\Delta U}_{s\mathrm{T}}) \end{aligned} \quad (57)$$

where

$$\mathbf{r}_f = \tilde{\mathbf{t}}_f^T \otimes (\mathbf{I}_M + \widetilde{\mathbf{U}}_{sT}\mathbf{D}_f) \quad (58)$$

because $\mathbf{\Delta z}_{f\mathrm{T}}$ is in fact a vector.

Based on the perturbation of $[\boldsymbol{\mathcal{Z}}_f]_{R+1}^{T}$ in (57) and (35), the mean of $\hat{\omega}_{r,f}$ has been derived as (see Appendix):

$$\mathbb{E}\{\hat{\omega}_{r,f}\} \approx \omega_{r,f} \quad (59)$$

which indicates that the TEV estimator is approximately unbiased. The corresponding mean square error or variance, denoted by $\mathrm{var}(\hat{\omega}_{r,f})$, is

$$\mathrm{var}(\hat{\omega}_{r,f}) \approx \frac{\sigma^2}{2\tilde{\lambda}_{r,f}^2}\left\|\mathbf{W}_{\mathrm{T}}^T\mathbf{r}_f^T\mathbf{L}_{r,f}^T\right\|_2^2 \quad (60)$$

where $\mathbf{W}_{\mathrm{T}}$ and $\mathbf{L}_{r,f}$ are defined in Appendix A. When FB averaging is utilized, (60) is modified as (61) in the top of next page [21],

$$\begin{aligned}&\mathrm{var}\left(\hat{\omega}_{r,f}^{(\mathrm{FB})}\right) \\ &\approx \frac{\sigma^2}{2\tilde{\lambda}_{r,f}^2}\Bigg(\left\|\mathbf{W}_{\mathrm{T}}^{(\mathrm{FB})^T}\mathbf{r}_f^{(\mathrm{FB})^T}\mathbf{L}_{r,f}^{(\mathrm{FB})^T}\right\|_2^2 \\ &\quad - \mathrm{Re}\left\{\left(\frac{\mathbf{L}_{r,f}^{(\mathrm{FB})}\mathbf{r}_f^{(\mathrm{FB})}\mathbf{W}_{\mathrm{T}}^{(\mathrm{FB})}}{\rho_{r,f}}\right)\right. \\ &\quad \left.\times\ \Pi_{2MN}\left(\frac{\mathbf{L}_{r,f}^{(\mathrm{FB})}\mathbf{r}_f^{(\mathrm{FB})}\mathbf{W}_{\mathrm{T}}^{(\mathrm{FB})}}{\rho_{r,f}}\right)^T\right\}\Bigg) \end{aligned} \quad (61)$$

where Re denotes the real part while $\mathbf{W}_{\mathrm{T}}^{(\mathrm{FB})}$, $\mathbf{r}_f^{(\mathrm{FB})}$ and $\mathbf{L}_{r,f}^{(\mathrm{FB})}$ are defined accordingly.

V. Numerical Examples

Computer simulations have been carried out to evaluate the performance of the proposed R-D HR approach by comparing with the unitary ESPRIT (UE) [14], unitary tensor ESPRIT (UTE) [15], and MDF [18] schemes as well as CRLB. Notice that the CRLB is derived in matrix forms in [17] and in scalar forms in [24], and that for identical frequencies given in [25]. Without considering the simultaneous Schur decomposition (SSD) step [14] for pairing up the frequencies in multiple dimensions, the major complexity orders of the UE [14] and UTE [15] methods are $\mathcal{O}(2k_tFMN)$ and $\mathcal{O}(2k_tF(R+1)MN)$, which are due to SVD and HOSVD, respectively. On the other hand, the main computational load of the MDF scheme has a complexity of $\mathcal{O}(2k_tK^EL^ENF)$ where $K^E = \prod_{r=1}^{R}K_r^E$, $L^E = \prod_{r=1}^{R}L_r^E$, $L_r^E + K_r^E - 1 = M_r$, $r = 1, 2, \cdots, R$, and typically $\prod_{r=1}^{R}(K_r^E - 1) \approx 2L^EN$ is employed. Furthermore, we choose $\kappa_r = 1$ for the SLS update in the TEV approach and consider the challenging case when identical frequencies appear in at least one dimension. The signal power vector of the F frequencies is defined as $\boldsymbol{\sigma}_\gamma^2 = [\sigma_1^2\ \sigma_2^2\ \cdots\ \sigma_F^2]$ and all elements in the noise tensor $\boldsymbol{\mathcal{Q}}$ are ZMCSCG processes with identical variances σ^2. Different signal-to-noise ratio (SNR) conditions are obtained by properly scaling $\boldsymbol{\mathcal{Q}}$ where $\mathrm{SNR} = \|\mathrm{vec}(\boldsymbol{\mathcal{S}})\|_2^2/(MN\sigma^2)$. All results provided are averages of 2000 independent runs.

Prior to the comparative study, we test the performance of the TEV method under different combinations of iteration numbers, namely, ι_1 and ι_2. Estimation of 6 frequency pairs from a 10×10 data set with $N = 10$ snapshots for each point, which is in fact a 3-D estimation problem, is considered. The signal power vector is$\boldsymbol{\sigma}_\gamma^2 = [2\ 3\ 2\ 3\ 2\ 3]$ while the frequencies are $[\omega_{1,1}\ \omega_{1,2}\ \omega_{1,3}\ \omega_{1,4}\ \omega_{1,5}\ \omega_{1,6}] = [0.1\pi\ \ 0.2\pi\ \ 0.2\pi\ \ 0.6\pi\ \ 0.1\pi\ \ 0.6\pi]$ and $[\omega_{2,1}\,\omega_{2,2}\,\omega_{2,3}\,\omega_{2,4}\,\omega_{2,5}\,\omega_{2,6}] = [0.1\pi\,0.1\pi\,0.3\pi\,0.3\pi\,0.5\pi\,0.5\pi]$. The average mean square frequency error (AMSFE) performance versus SNR is shown in Fig. 1. The theoretical calculation of (60) and the benchmark of CRLB are also included. Note that $\iota_1 = 0$ corresponds to the LS solution and there is no SLS step while $\iota_2 = 1$ refers to a randomly selected $\boldsymbol{\alpha}$ in Table I. With the choice of $\iota_1 = 1$ and $\iota_2 = 2$, the estimator is able to attain the theoretical bound for sufficiently high SNR, namely, $\mathrm{SNR} > 15$ dB, and no obvious improvement is observed for larger iteration numbers. As a result, we employ $\iota_1 = 1$ and $\iota_2 = 2$, which also align with [13] and [18], respectively, in the subsequent tests. Moreover, the AMSFE is larger than the CRLB by about 5 dB under small error conditions. Recall that the major computational requirement of the TEV method is $\mathcal{O}(k_tF(R+1)MN) + \mathcal{O}(k_tFM\iota_2) + \mathcal{O}(F\iota_1\sum_{r=1}^{R}M_r^3)$. This means that if we employ the LS estimate, the last term will be zero. Nevertheless, it is seen that when R is sufficiently large, the first and second terms dominate, indicating that the complexities of the LS and SLS solutions are comparable in this scenarios.

In the second experiment, the proposed methods which include the FB averaging version, denoted by TEV-FB, are compared with the UE, UTE, and MDF schemes. We keep using

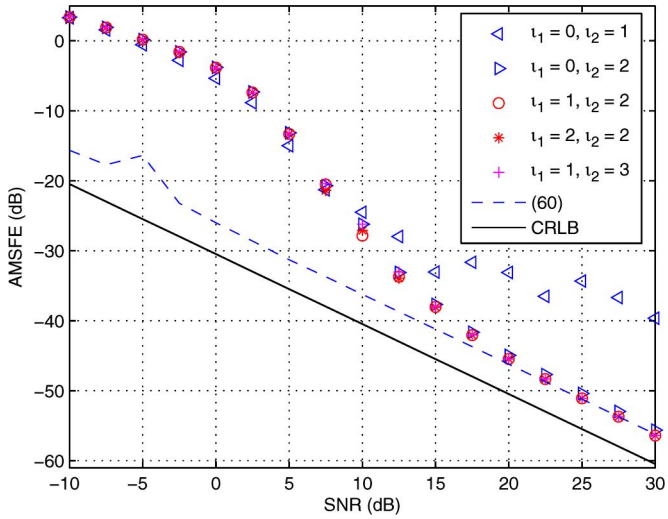

Fig. 1. Average mean square frequency error versus SNR at different ι_1 and ι_2.

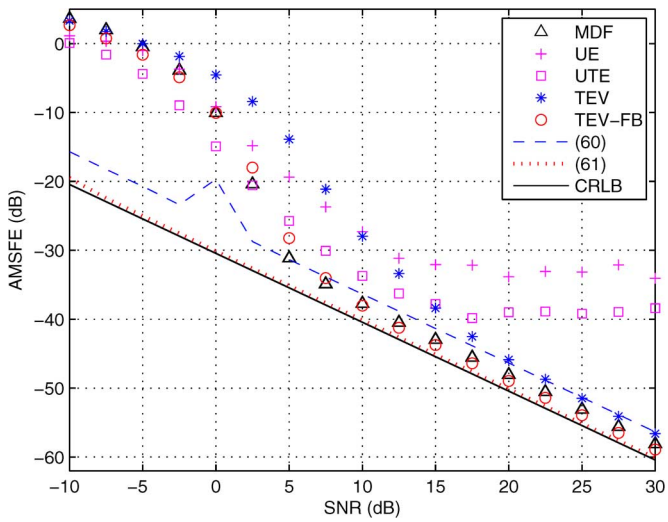

Fig. 2. Average mean square frequency error versus SNR at $M_1 = M_2 = N = 10$ and $F = 6$.

the previous parameter settings. The AMSFEs versus SNR are plotted in Fig. 2. It is seen that the TEV-FB method has the best performance at SNR $>$ 10 dB while the corresponding AMSFE agrees with (61) and is close to the CRLB. As expected, it can attain higher estimation accuracy than the standard TEV estimator. Furthermore, we observe the poor performance of the UE and UTE methods at sufficiently high SNR conditions, which might be due to the erroneous frequency pairing step based on SSD. On the other hand, the average computation times of the MDF, UE, UTE, TEV and TEV-FB algorithms in a single run are measured as 0.0355 s, 0.0620 s, 0.0087 s, 0.0052 s and 0.0059 s, respectively, indicating the computational attractiveness of the TEV approach.

The third test examines another challenging 2-D HR setting where the frequencies are very close in the first dimension and are identical in the second dimension. We consider a smaller array of $M_1 = M_2 = 8$ while a larger snapshot length of $N = 50$. The signal parameters are

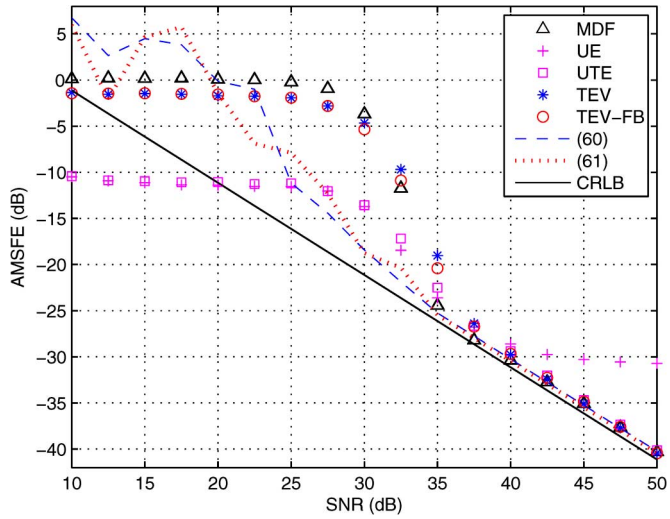

Fig. 3. Average mean square frequency error versus SNR at $M_1 = M_2 = 8$, $N = 50$ and $F = 4$.

$\boldsymbol{\sigma}_\gamma^2 = [2\ 3\ 2\ 3]$, $[\omega_{1,1}\ \omega_{1,2}\ \omega_{1,3}\ \omega_{1,4}] = [0.1\pi\ 0.15\pi\ 0.2\pi\ 0.25\pi]$ and $[\omega_{2,1}\ \omega_{2,2}\ \omega_{2,3}\ \omega_{2,4}] = [0.1\pi\ 0.1\pi\ 0.1\pi\ 0.1\pi]$. The AMSFEs versus SNR are plotted in Fig. 3. At SNR $>$ 35 dB, the proposed methods as well as the MDF and UTE estimators perform comparably to the CRLB and are superior to the UE scheme. That is to say, there is no improvement when forward-backward averaging is utilized, probably because the number of snapshots is already large enough. Moreover, the UE method is inferior to the UTE scheme for high SNRs, which implies the advantage of exploiting the tensor structure. Nevertheless, the MDF method has the minimum threshold SNR of 35 dB. The theoretical calculations of (60) and (61) are also confirmed. Furthermore, the average computation times of the MDF, UE, UTE, TEV and TEV-FB algorithms are 0.0407 s, 0.0218 s, 0.0141 s, 0.0058 s and 0.0104 s, respectively. As a result, the TEV estimator is the best choice in terms of accuracy and computational efficiency for large snapshot scenarios.

In the fourth test, we study 3-D HR with single snapshot or $N = 1$. The signal size is $M_1 = M_2 = M_3 = 10$ and the signal power vector is identical to that in the previous test. The frequencies are $[\omega_{1,1}\ \omega_{1,2}\ \omega_{1,3}\ \omega_{1,4}] = [0.1\pi\ 0.13\pi\ 0.16\pi\ 0.19\pi]$, $[\omega_{2,1}\ \omega_{2,2}\ \omega_{2,3}\ \omega_{2,4}] = [0.1\pi\ 0.3\pi\ 0.3\pi\ 0.1\pi]$ and $[\omega_{2,1}\ \omega_{2,2}\ \omega_{2,3}\ \omega_{2,4}] = [0.1\pi\ 0.1\pi\ 0.4\pi\ 0.4\pi]$. From now on, we do not include the UE method in the comparison because it is inferior to the UTE algorithm. The AMSFEs are plotted in Fig. 4 and we observe that the TEV-FB method performs the best, followed by the UTE scheme. On the other hand, the performance of the TEV and MDF methods is not satisfactory for all SNRs. Note that since spatial smoothing is required, the noise in the resultant HOSVD is no longer uncorrelated. As a result, the variance expressions will be more complicated than (60) and (61) and they are not provided. Together with the average computation times of the MDF, UTE, TEV and TEV-FB algorithms, which are 0.0719 s, 0.0612 s, 0.0170 s and 0.0323 s, respectively, we deduce that the TEV-FB estimator is an optimal choice in this case.

The fifth test investigates 3-D single-tone estimation where the signal is the first tone in the previous experiment. The data

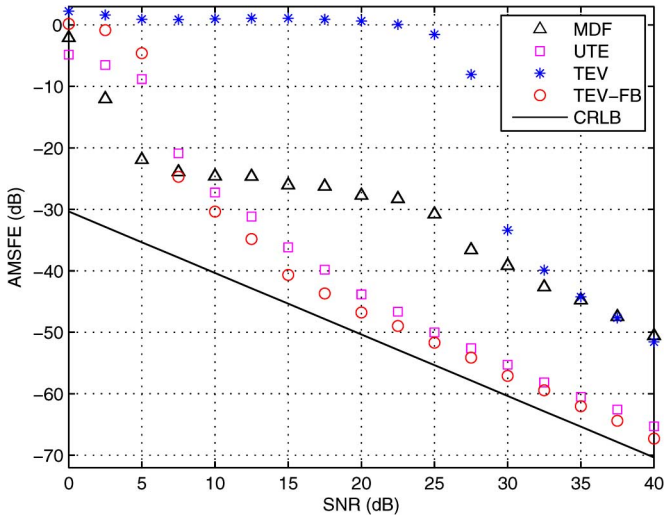

Fig. 4. Average mean square frequency error versus SNR at $M_1 = M_2 = M_3 = 10$, $N = 1$ and $F = 4$.

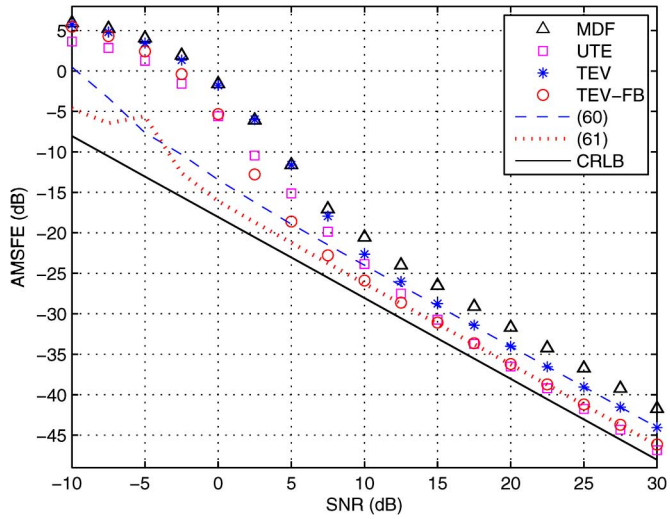

Fig. 6. Average mean square frequency error versus SNR at $M_1 = M_2 = M_3 = 3$, $N = 10$ and $F = 4$.

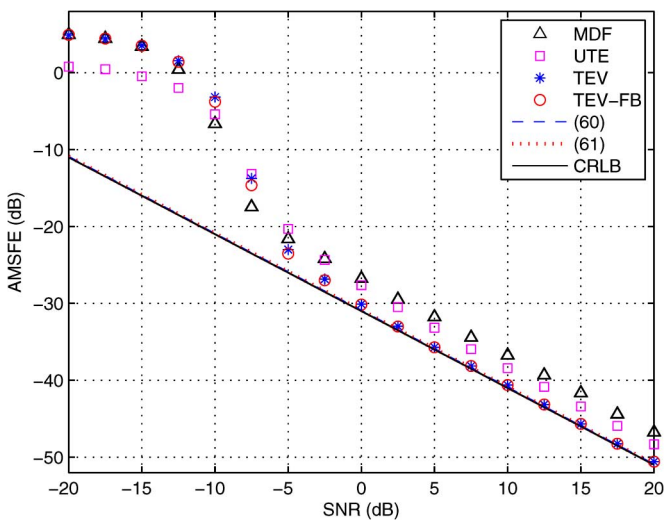

Fig. 5. Average mean square frequency error versus SNR at $M_1 = M_2 = M_3 = 6$ and $N = F = 1$.

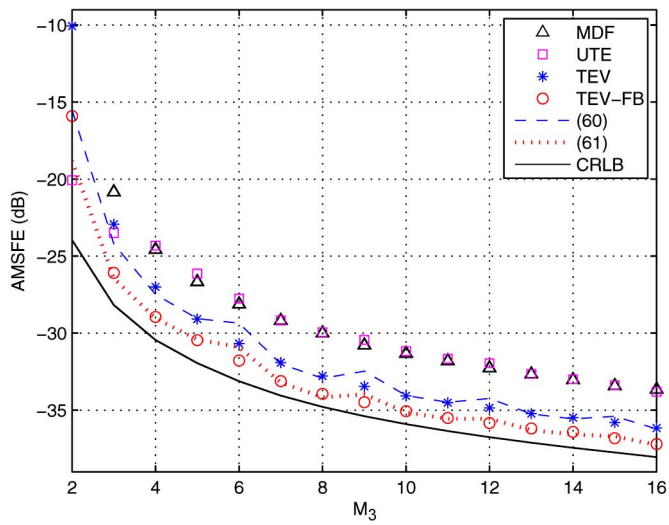

Fig. 7. Average mean square frequency error versus M_3.

size is $6 \times 6 \times 6$ with $N = 1$ and the results are shown in Fig. 5. We see that the proposed methods have optimum performance when SNR $\geq$ 0 dB and are superior to the MDF and UTE estimators. Again, (60) and (61) are validated. Note that when $F = 1$, the update of $\boldsymbol{\alpha}$ is not needed and the received data tensor has the form of $\boldsymbol{\mathcal{Z}}_1$ in (32), and thus the TEV approach can be further simplified. On the other hand, the average computation times of the MDF, UTE, TEV and TEV-FB algorithms are measured as 0.0058 s, 0.0040 s, 0.0012 s and 0.0019 s.

In the sixth experiment, we examine a 3-D case of $F > \max\{M_1, M_2, \cdots, M_R\}$ where $F = 4$ while $M_1 = M_2 = M_3 = 3$ and $N = 10$. The signal power vector is the same as that of the fourth test and the frequencies are $[\omega_{1,1}\ \omega_{1,2}\ \omega_{1,3}\ \omega_{1,4}] = [0.1\pi\ 0.6\pi\ 0.1\pi\ 0.6\pi]$, $[\omega_{2,1}\ \omega_{2,2}\ \omega_{2,3}\ \omega_{2,4}] = [-0.1\pi\ 0.1\pi\ -0.6\pi\ 0.6\pi]$ and $[\omega_{2,1}\ \omega_{2,2}\ \omega_{2,3}\ \omega_{2,4}] = [0.1\pi\ 0.3\pi\ 0.6\pi\ 0.9\pi]$. The corresponding AMSFE performance is plotted in Fig. 6. It is seen that the TEV-FB and UTE methods perform similarly but the former has a smaller threshold SNR, and they are superior to the remaining two schemes. We also see that (60) and (61) agree with the numerical results for sufficiently high SNR conditions. In addition, the average computation times of the MDF, UTE, TEV and TEV-FB algorithms are 0.0031 s, 0.0237 s, 0.0123 s and 0.0132 s, respectively.

In the final test, the performance versus $M_3 \in [2, 16]$ at SNR $=$ 10 dB is studied to evaluate the impact of $\mathcal{O}(F\iota_1 \sum_{r=1}^{R} M_r^3)$ in the complexity of the proposed approach. All other parameter settings are identical to those of the previous experiment. The AMSFE and runtime results are plotted in Figs. 7 and 8, respectively. In Fig. 7, it is observed that the TEV-FB algorithm gives the best estimation performance. While Fig. 8 shows that the complexity of the TEV approach increases linearly with M_3, indicating that the combined term of $\mathcal{O}(k_t F(R+1)MN) + \mathcal{O}(k_t F M \iota_2)$ dominates $\mathcal{O}(F\iota_1 \sum_{r=1}^{R} M_r^3)$. Although the MDF scheme is the most computationally attractive for small M_3, its complexity is higher than that of the TEV-FB algorithm when $M_3 \geq 15$.

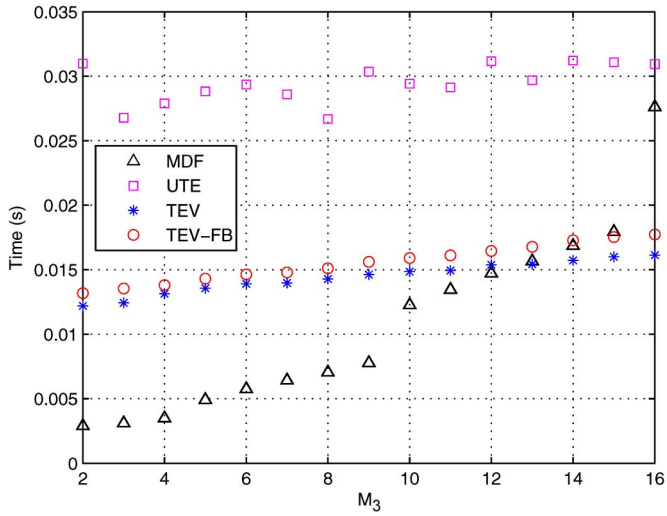

Fig. 8. Average computational time versus M_3.

VI. Conclusion

A subspace-based approach for R-dimensional (R-D) harmonic retrieval even in the presence of identical frequencies is devised. With the use of higher-order singular value decomposition, the received tensor of F R-D sinusoids is broken down into RF vectors where each of them corresponds to a 1-D single-tone sequence. Each frequency is then accurately retrieved using the structured least squares technique. The bias and variance of the subspace-based method are also analyzed and it is proved that the frequency estimates are approximately unbiased. Computer simulations show that the proposed algorithm is computationally simpler than conventional HR estimators and can provide superior estimation performance.

Appendix A

We first show that the TEV estimator is approximately unbiased and then derive the variance for $\hat{\omega}_{r,f}$.

According to (35) and [23], we have

$$\begin{aligned}\Delta\mathbf{h}_{r,f} &= (\mathbf{I}_{M_r} - \tilde{\mathbf{h}}_{r,f}\tilde{\mathbf{h}}_{r,f})^H)[\Delta\boldsymbol{\mathcal{Z}}_f]_{(r)}\tilde{\mathbf{v}}_{r,f}\tilde{\lambda}_{r,f}^{-1} \\ &= \tilde{\lambda}_{r,f}^{-1}\left[\tilde{\mathbf{v}}_{r,f}^T \otimes (\mathbf{I}_{M_r} - \tilde{\mathbf{h}}_{r,f}\tilde{\mathbf{h}}_{r,f})^H)\right]\mathrm{vec}\left([\Delta\boldsymbol{\mathcal{Z}}_f]_{(r)}\right) \\ &= \tilde{\lambda}_{r,f}^{-1}\mathbf{L}_{r,f,1}\mathbf{K}_r^T[\Delta\boldsymbol{\mathcal{Z}}_f]_{(R+1)} \\ &= \tilde{\lambda}_{r,f}^{-1}\mathbf{L}_{r,f,1}\mathbf{K}_r^T\Delta\mathbf{z}_{Tf} \end{aligned} \tag{A.1}$$

where $\mathbf{L}_{r,f,1} = \tilde{\mathbf{v}}_{r,f}^T \otimes (\mathbf{I}_{M_r} - \tilde{\mathbf{h}}_{r,f}\tilde{\mathbf{h}}_{r,f})^H)$ and $\mathbf{K}_r$ is a selection matrix such that $[\Delta\boldsymbol{\mathcal{Z}}_f]_{(R+1)} = \mathbf{K}_r\mathrm{vec}([\Delta\boldsymbol{\mathcal{Z}}_f]_{(r)})$. Notice that $\mathbf{K}_r$ is a sparse matrix with entries 0 or 1 and $\mathbf{K}_r\mathbf{K}_r^T = \mathbf{I}_M$.

The final estimate $\hat{\rho}_{r,f}$ in (44) can be written as:

$$\hat{\rho}_{r,f} = \hat{\rho}_{r,f|_0} + \Delta\rho_{r,f}^{\mathrm{SLS}} = \tilde{\rho}_{r,f} + \Delta\rho_{r,f|_0} + \Delta\rho_{r,f}^{\mathrm{SLS}} \tag{A.2}$$

That is, the total error term $\Delta\rho_{r,f}$ consists of $\Delta\rho_{r,f|_0}$ from the LS estimation and $\Delta\rho_{r,f}^{\mathrm{SLS}}$ from the SLS update. According to [26], the estimation error of the LS estimate at $\iota_1 = 0$ is:

$$\Delta\rho_{r,f|_0} = (\mathbf{J}_{1,r}\tilde{\mathbf{h}}_{r,f})^\dagger(\mathbf{J}_{2,r} - \mathbf{J}_{1,r}\tilde{\rho}_{r,f})\Delta\mathbf{h}_{r,f} \tag{A.3}$$

For the case when $\iota_1 > 0$, we follow [27] and set $\kappa_r = 0$ in (38), which means that only minimization of $\|\mathbf{R}(\rho_{r,f}, \mathbf{h}_{r,f}^i)\|_2$ is considered. Under sufficiently small noise conditions, solving (38) yields

$$\begin{bmatrix}\Delta\rho_{r,f}^{\mathrm{SLS}} \\ \Delta\mathbf{h}_{r,f}\end{bmatrix} = \mathbf{F}_{r,f}^\dagger\mathbf{r}_{r,f} \approx \widetilde{\mathbf{F}}_{r,f}^\dagger\mathbf{r}_{r,f} \tag{A.4}$$

where

$$\mathbf{F}_{r,f} = [\mathbf{J}_{1,r}\mathbf{h}_{r,f} \quad \mathbf{J}_{1,r}\rho_{r,f} - \mathbf{J}_{2,r}] \tag{A.5}$$

$$\begin{aligned}\mathbf{r}_{r,f} &= \mathbf{J}_{1,r}(\tilde{\mathbf{h}}_{r,f} + \Delta\mathbf{h}_{r,f})(\tilde{\rho}_{r,f} + \Delta\rho_{r,f|_0}) \\ &\quad - \mathbf{J}_{2,r}(\tilde{\mathbf{h}}_{r,f} + \Delta\mathbf{h}_{r,f}) \\ &= \mathbf{W}_{r,f}\Delta\mathbf{h}_{r,f}\end{aligned} \tag{A.6}$$

$$\begin{aligned}\mathbf{W}_{r,f} = &\left(\mathbf{J}_{1,r}\tilde{\mathbf{h}}_{r,f}(\mathbf{J}_{1,r}\tilde{\mathbf{h}}_{r,f})^\dagger - \mathbf{I}_{M_r-1}\right) \\ &\times (\mathbf{J}_{2,r} - \mathbf{J}_{1,r}\tilde{\rho}_{r,f})\end{aligned} \tag{A.7}$$

On the other hand, combining (A.4)–(A.7) $\Delta\rho_{r,f}^{\mathrm{SLS}}$ is

$$\Delta\rho_{r,f}^{\mathrm{SLS}} = \mathbf{W}_{r,f,2}\mathbf{W}_{r,f}\Delta\mathbf{h}_{r,f} \tag{A.8}$$

where

$$\mathbf{W}_{r,f,2} = (\mathbf{J}_{1,r}\tilde{\mathbf{h}}_{r,f})^H\left(\widetilde{\mathbf{F}}_{r,f}\widetilde{\mathbf{F}}_{r,f}^H\right)^{-1} \tag{A.9}$$

Employing (A.3) and (A.8), the total estimation error in $\hat{\rho}_{r,f}$ is:

$$\Delta\rho_{r,f} = \Delta\rho_{r,f|_0} + \Delta\rho_{r,f}^{\mathrm{SLS}} = \tilde{\lambda}_{r,f}^{-1}\mathbf{L}_{r,f}\Delta\mathbf{z}_{f\mathrm{T}} \tag{A.10}$$

where

$$\mathbf{L}_{r,f} = \left[(\mathbf{J}_{1,r}\tilde{\mathbf{h}}_{r,f})^\dagger(\mathbf{J}_{2,r} - \mathbf{J}_{1,r}\tilde{\rho}_{r,f}) + \mathbf{W}_{r,f,2}\mathbf{W}_{r,f}\right]\mathbf{L}_{r,f,1}\mathbf{K}_r^T \tag{A.11}$$

From (57) and (A.10), we obtain

$$\Delta\rho_{r,f} = \tilde{\lambda}_{r,f}^{-1}\mathbf{L}_{r,f}\mathbf{r}_f\mathrm{vec}(\Delta\mathbf{U}_{s\mathrm{T}}) \tag{A.12}$$

Furthermore, using (48)–(50), $\mathrm{vec}(\Delta\mathbf{U}_{s\mathrm{T}})$ can be written as

$$\mathrm{vec}(\Delta\mathbf{U}_{s\mathrm{T}}) = \mathbf{W}_{\mathrm{T}}\mathrm{vec}\left\{[\boldsymbol{\mathcal{Q}}]_{R+1}^T\right\} \tag{A.13}$$

where

$$\begin{aligned}\mathbf{W}_{\mathrm{T}} = &\widetilde{\mathbf{U}}_{R+1}^{[s]^H} \otimes \left[\left(\widetilde{\Upsilon}_1 \otimes \widetilde{\Upsilon}_2 \otimes \cdots \otimes \widetilde{\Upsilon}_R\right)\widetilde{\mathbf{V}}_{R+1}^{[n]^*}\widetilde{\mathbf{V}}_{R+1}^{[n]^T}\right] \\ &+ \sum_{r=1}^{R}\widetilde{\mathbf{P}}_r\end{aligned} \tag{A.14}$$

$$\begin{aligned}\widetilde{\mathbf{P}}_r = &\left(\widetilde{\boldsymbol{\Sigma}}_{R+1}^{[s]}\widetilde{\mathbf{V}}_{R+1}^{[s]^H} \otimes \mathbf{I}_M\right)\widetilde{\mathbf{B}}_{r1}\widetilde{\mathbf{B}}_{r2} \\ &\times \left[\left(\widetilde{\mathbf{U}}_r^{[s]^*}\widetilde{\boldsymbol{\Sigma}}_r^{[s]}\widetilde{\mathbf{V}}_r^{[s]^T}\right) \otimes \left(\widetilde{\mathbf{U}}_r^{[n]}\widetilde{\mathbf{U}}_r^{[n]^H}\right)\right]\mathbf{K}_r^{\vdash^T}\end{aligned} \tag{A.15}$$

$$\mathbf{B}_{r1} = \begin{bmatrix}\mathbf{I}_{N_{r2}} \otimes \mathbf{t}_{r1,1} \otimes \mathbf{I}_{N_{r2}} \\ \mathbf{I}_{N_{r2}} \otimes \mathbf{t}_{r1,2} \otimes \mathbf{I}_{N_{r2}} \\ \vdots \\ \mathbf{I}_{N_{r2}} \otimes \mathbf{t}_{r1,N_{r1}} \otimes \mathbf{I}_{N_{r2}}\end{bmatrix} \tag{A.16}$$

$$\mathbf{B}_{r2}=\mathbf{I}_{M_r}\otimes\begin{bmatrix}\mathbf{I}_{M_r}\otimes\mathbf{t}_{r2,1}\\ \mathbf{I}_{M_r}\otimes\mathbf{t}_{r2,2}\\ \vdots\\ \mathbf{I}_{M_r}\otimes\mathbf{t}_{r2,N_{r2}}/M_r\end{bmatrix} \tag{A.17}$$

with $N_{r1}=\prod_{i=1}^{r-1}M_i$, $N_{r2}=\prod_{i=r}^{R}M_i$, $\mathbf{T}_{r1}=\Upsilon_1\otimes\Upsilon_2\otimes\cdots\otimes\Upsilon_{r-1}$, $\mathbf{T}_{r2}=\Upsilon_{r+1}\otimes\Upsilon_{r+2}\otimes\cdots\otimes\Upsilon_R$. The $\mathbf{t}_{r1,i}$ and $\mathbf{t}_{r2,j}$ are the ith and jth columns of $\mathbf{T}_{r1}$ and $\mathbf{T}_{r2}$, and $\mathbf{K}_r^{\vdash}$ is a highly sparse selection matrix with entries 0 or 1 such that $\mathrm{vec}([\boldsymbol{\Delta}\boldsymbol{\mathcal{Q}}]_{(R+1)}^T)=\mathbf{K}_r^{\vdash^T}\mathrm{vec}([\boldsymbol{\mathcal{Q}}]_{(r)})$ for any $\boldsymbol{\mathcal{Q}}$ and $\mathbf{K}_r^{\vdash}\mathbf{K}_r^{\vdash^T}=\mathbf{I}_{MN}$.

Using (A.12), (A.13) and (2), we have $\mathbb{E}\{\mathrm{vec}\{[\boldsymbol{\mathcal{Q}}]_{R+1}^T\}\}=\mathbf{0}_{MN\times 1}$, $\mathbb{E}\{\mathrm{vec}\{[\boldsymbol{\mathcal{Q}}]_{R+1}^T\}\mathrm{vec}\{[\boldsymbol{\mathcal{Q}}]_{R+1}^T\}^H\}=\sigma^2\mathbf{I}_{MN}$ and $\rho_{r,f}^H\rho_{r,f}=1$. Together with $\Delta\omega_{r,f}=\mathrm{Im}\{\Delta\rho_{r,f}\}/\rho_{r,f}$ [26], where Im denotes the imaginary part. The approximate unbiasedness of $\hat{\omega}_{r,f}$ is thus proved. Moreover, we obtain

$$\begin{aligned}\mathbb{E}(\Delta\hat{\omega}_{r,f}^2)=&\frac{1}{2}\tilde{\lambda}_{r,f}^{-2}\left(\frac{\mathbf{L}_{r,f}\mathbf{r}_f\mathbf{W}_{\mathrm{T}}}{\rho_{r,f}}\right)\\ &\times\mathbb{E}\left\{\mathrm{vec}\left\{[\boldsymbol{\mathcal{Q}}]_{R+1}^T\right\}\mathrm{vec}\left\{[\boldsymbol{\mathcal{Q}}]_{R+1}^T\right\}^H\right\}\\ &\times\left(\frac{\mathbf{L}_{r,f}\mathbf{r}_f\mathbf{W}_{\mathrm{T}}}{\rho_{r,f}}\right)^H\end{aligned} \tag{A.18}$$

which can be reduced to (60).

REFERENCES

[1] P. Stoica and R. Moses, *Spectral Analysis of Signals*. Upper Saddle River, NJ, USA: Prentice-Hall, 2005.

[2] K. T. Wong and M. D. Zoltowski, "Uni-vector-sensor ESPRIT for multisource azimuth-elevation angle estimation," *IEEE Trans. Antennas Propag.*, vol. 45, no. 10, pp. 1467–1474, Oct. 1997.

[3] M. Pesavento, C. F. Mecklenbrauker, and J. F. Bohme, "Multidimensional rank-reduction estimator for parametric MIMO channel models," *EURASIP J. Appl. Signal Process.*, pp. 1354–1363, Aug. 2004.

[4] X. Liu, N. D. Sidiropoulos, and T. Jiang, "Multidimensional harmonic retrieval with applications in MIMO wireless channel sounding," in *Space-Time Processing for MIMO Communications*, A. B. Gershman and N. D. Sidiropoulos, Eds. New York, NY, USA: Wiley, 2005.

[5] A. Bax, "A simple description of two-dimensional NMR spectroscopy," *Bull. Magn. Reson.*, vol. 7, pp. 167–183, 1985.

[6] Y. Li, J. Razavilar, and K. J. R. Liu, "A high-resolution technique for multidimensional NMR spectroscopy," *IEEE Trans. Biomed. Eng.*, vol. 45, no. 1, pp. 78–86, Jan. 1998.

[7] D. Nion and N. D. Sidiropoulos, "A PARAFAC-based technique for detection and localization of multiple targets in a MIMO radar system," in *Proc. IEEE Int. Conf. Acoust., Speech, Signal Process. (ICASSP)*, Taipei, Taiwan, Apr. 2009, pp. 2077–2080.

[8] D. Nion and N. D. Sidiropoulos, "Tensor algebra and multidimensional harmonic retrieval in signal processing for MIMO radar," *IEEE Trans. Signal Process.*, vol. 58, no. 11, pp. 5693–5705, Nov. 2010.

[9] L. de Lathauwer, B. de Moor, and J. Vanderwalle, "A multilinear singular value decomposition," *SIAM J. Matrix Anal. Appl.*, vol. 21, no. 4, pp. 1253–1278, 2000.

[10] L. de Lathauwer, B. de Moor, and J. Vanderwalle, "On the best rank-1 and rank- $(r_1, r_2, \ldots, r_n)$ approximation of higher-order tensors," *SIAM J. Matrix Anal. Appl.*, vol. 21, no. 4, pp. 1324–1342, 2000.

[11] T. G. Kolda and B. W. Bader, "Tensor decompositions and applications," *SIAM Rev.*, vol. 51, no. 3, pp. 455–500, Sep. 2009.

[12] M. Haardt and J. A. Nossek, "Unitary ESPRIT: How to obtain increased estimation accuracy with a reduced computational burden," *IEEE Trans. Signal Process.*, vol. 43, no. 5, pp. 1232–1242, May 1995.

[13] M. Haardt, "Structured least squares to improve the performance of ESPRIT-type algorithms," *IEEE Trans. Signal Process.*, vol. 45, no. 3, pp. 792–799, Mar. 1997.

[14] M. Haardt and J. A. Nossek, "Simultaneous Schur decomposition of several nonsymmetric matrices to achieve automatic pairing in multidimensional harmonic retrieval problems," *IEEE Trans. Signal Process.*, vol. 46, no. 1, pp. 161–169, Jan. 1998.

[15] M. Haardt, F. Roemer, and G. Del Galdo, "Higher-order SVD-based subspace estimation to improve the parameter estimation accuracy in multidimensional harmonic retrieval problems," *IEEE Trans. Signal Process.*, vol. 56, no. 7, pp. 3198–3213, Jul. 2008.

[16] A. Thakre, M. Haardt, F. Roemer, and K. Giridhar, "Tensor-based spatial smoothing (TB-SS) using multiple snapshots," *IEEE Trans. Signal Process.*, vol. 58, no. 5, pp. 2715–2728, May 2010.

[17] J. Liu and X. Liu, "An eigenvector-based approach for multidimensional frequency estimation with improved identifiability," *IEEE Trans. Signal Process.*, vol. 54, no. 12, pp. 4543–4556, Dec. 2006.

[18] J. Liu, X. Liu, and X. Ma, "Multidimensional frequency estimation with finite snapshots in the presence of identical frequencies," *IEEE Trans. Signal Process.*, vol. 55, no. 11, pp. 5179–5194, Nov. 2007.

[19] H. C. So, F. K. W. Chan, W. H. Lau, and C. F. Chan, "An efficient approach for two-dimensional parameter estimation of a single-tone," *IEEE Trans. Signal Process.*, vol. 58, no. 4, pp. 1999–2009, Apr. 2010.

[20] W. Sun and H. C. So, "Accurate and computationally efficient tensor-based subspace approach for multi-dimensional harmonic retrieval," *IEEE Trans. Signal Process.*, vol. 60, no. 10, pp. 5077–5088, Oct. 2012.

[21] F. Roemer, H. Becker, M. Haardt, and M. Weis, "Analytical performance evaluation for HOSVD-based parameter estimation schemes," in *Proc. Int. Workshop Comp. Adv. in Multi-Sensor Adapt. Process. (CAMSAP)*, Aruba, Dutch Antilles, Dec. 2009, pp. 77–80.

[22] G. H. Golub and C. F. van Loan, *Matrix Computations*. Baltimore, MD, USA: The John Hopkins Univ. Press, 1996.

[23] J. Liu, X. Liu, and X. Ma, "First-order perturbation analysis of singular vectors in singular value decomposition," *IEEE Trans. Signal Process.*, vol. 56, no. 7, pp. 3044–3049, Jul. 2008.

[24] R. Boyer, "Deterministic asymptotic Cramér-Rao bound for the multidimensional harmonic model," *Signal Process.*, vol. 88, no. 12, pp. 2869–2877, Dec. 2008.

[25] N. Sajlad and R. Boyer, "Asymptotic Cramér-Rao bound for multidimensional harmonic models," in *Proc. IEEE Int. Conf. Acoust., Speech, Signal Process. (ICASSP)*, Honolulu, HI, USA, Apr. 2007, pp. 1041–1044.

[26] F. Li, H. Liu, and R. J. Vaccaro, "Performance analysis for DOA estimation algorithms: Unification, simplifications, observations," *IEEE Trans. Aerosp. Electron. Syst.*, vol. 29, no. 4, pp. 1170–1184, Oct. 1993.

[27] F. Roemer and M. Haardt, "Analytical performance assessment of 1-D structured least squares," in *Proc. IEEE Int. Conf. Acous., Speech, Signal Process. (ICASSP)*, Prague, Czech, May 2011, pp. 2464–2467.

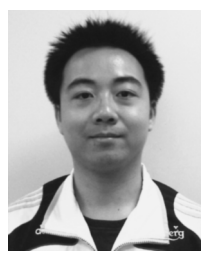

Weize Sun received the B.S. degree in Electronic Information Science and Technology from Sun Yat-Sen University, China, in 2009. He is currently a Research Student and working towards his Ph.D. degree in City University of Hong Kong. His research interests include statistical signal processing, parameter estimation, tensor algebra, with particular attention to frequency estimation.

Hing Cheung So (S'90–M'95–SM'07) was born in Hong Kong. He received the B.Eng. degree from the City University of Hong Kong and the Ph.D. degree from The Chinese University of Hong Kong, both in electronic engineering, in 1990 and 1995, respectively. From 1990 to 1991, he was an Electronic Engineer with the Research and Development Division, Everex Systems Engineering Ltd., Hong Kong. During 1995–1996, he worked as a Postdoctoral Fellow with The Chinese University of Hong Kong. From 1996 to 1999, he was a Research Assistant Professor with the Department of Electronic Engineering, City University of Hong Kong, where he is currently an Associate Professor. His research interests include statistical signal processing, fast and adaptive algorithms, signal detection, parameter estimation, and source localization.

Dr. So has been on the editorial boards of the IEEE TRANSACTIONS ON SIGNAL PROCESSING, *Signal Processing*, *Digital Signal Processing*, and *ISRN Applied Mathematics*, as well as a member of the Signal Processing Theory and Methods Technical Committee of the IEEE Signal Processing Society.

Frankie Kit Wing Chan received the B.Eng. degree in computer engineering and the Ph.D. degree in electronic engineering from the City University of Hong Kong in 2002 and 2008, respectively. He is currently a Research Fellow in the same university. His research interests include parameter estimation, optimization and distributed processing, with particular attention to frequency estimation, MIMO radar signal processing and node localization in wireless sensor network.

Lei Huang (M'07) was born in Guangdong, China. He received the B.Sc., M.Sc., and Ph.D. degrees in electronic engineering from Xidian University, Xian, China, in 2000, 2003, and 2005, respectively.

From 2005 to 2006, he was a Research Associate with the Department of Electrical and Computer Engineering, Duke University, Durham, NC. From 2009 to 2010, he was a Research Fellow with the Department of Electronic Engineering, City University of Hong Kong and a Research Associate with the Department of Electronic Engineering, The Chinese University of Hong Kong. Since 2011, he has joined the Department of Electronic and Information Engineering, Harbin Institute of Technology Shenzhen Graduate School, where he is currently a Professor. His research interests include spectral estimation, array signal processing, statistical signal processing, and their applications in radar and wireless communication systems.

He currently is an editorial board member of *Digital Signal Processing*.